Yield hardening of electrorheological fluids in channel flow

Ahmed Helal,[1] Bian Qian,[1] Gareth H. McKinley,[1] and A.E. Hosoi[1]

[1] *Hatsopoulos Microfluids Laboratory, Department of Mechanical Engineering, Massachusetts Institute of Technology, 77 Massachusetts Avenue, Cambridge, Massachusetts 02139, USA. Email: ahelal@mit.edu; Fax: +1 617-253-8559; Tel: +1 617-253-4337*

(Dated: December 15, 2015)

Electrorheological fluids offer potential for developing rapidly-actuated hydraulic devices where shear forces or pressure-driven flow are present. In this study, the Bingham yield stress of electrorheological fluids with different particle volume fractions was investigated experimentally in wall-driven and pressure-driven flow modes using measurements in a parallel-plate rheometer and a microfluidic channel, respectively. A modified Krieger-Dougherty model can be used to describe the effects of the particle volume fraction on the yield stress and is in good agreement with the viscometric data. However, significant yield-hardening in pressure-driven channel flow was observed and attributed to an increase, and eventual saturation, of the particle volume fraction in the channel. A phenomenological physical model linking the densification and consequent microstructure to the ratio of the particle aggregation time scale to the convection time scale is presented and is used to predict the enhancement in yield stress in channel flow, and enabling us to reconcile discrepancies in the literature between wall-driven and pressure-driven flows.

I. INTRODUCTION

Electrorheological (ER) fluids are materials that exhibit a reversible change in rheological properties with the application of an external electric field [1]. They consist, typically, of a suspension of dielectric particles in an insulating carrier fluid. When an electric field is applied, the particles aggregate and align in the direction of the field, forming columns consisting of chains of particles, which cause the fluid to transition from a liquid-like to a soft solid-like state. This change in the fluid properties is very rapid (on the order of tens of milliseconds) and is reversible upon removal of the electric field. These features have made ER fluids a promising candidate for use in a variety of hydraulic components and microfluidic devices including valves, clutches and dampers. Devices based on ER fluids can operate under three different modes: shear, flow and squeeze [2]. In shear mode, one of the electrodes is free to move in its plane, and common applications include clutches, brakes and dampers [3]. In flow mode, the electrodes are fixed and the pressure drop across the channel is controlled using the electric field. Valves and vibrators are typical applications in which ER fluids are used in flow mode [4–6]. In squeeze mode, the electrode gap is varied and the fluid is compressed in the wall-normal direction. Vibration control, shock absorbers and dampers are examples of application of ER fluids used in squeeze mode [2, 3]. A summary of the different modes of operation and their typical engineering applications is shown in Table 1. For each mode of operation, the particle interaction and the particle structures that are formed affect the mechanical properties of the ER fluid; most notably its yield strength, thus an understanding of the structures that form is crucial to predicting the mechanical performance of devices utilizing ER fluids. In shear mode, shear-induced lamellar structures are known to form while in flow mode, the structure tends to contain clusters and aggregates [7–9]. In addition, an enhancement in the shear yield strength has been shown in magnetorheological fluids as the fluid is compressed in the direction orthogonal to shear [10] and a strengthening of the microstructure of ER fluids has also been shown in squeeze mode by Tian et al [11].

The rheological response of ER fluids under shear is traditionally modeled using a continuum approach with a Bingham plastic model, where the application of the field induces a field-dependent yield stress [4]. The rheological constitutive relation for the ER fluid is typically expressed as:

$$\begin{aligned} \dot{\gamma} = 0 \quad & \text{if} \quad \tau < \tau_y(E,\phi) \\ \tau = \tau_y + \mu\dot{\gamma} \quad & \text{if} \quad \tau > \tau_y(E,\phi) \end{aligned} \tag{1}$$

where τ is the shear stress, $\dot{\gamma}$ the shear rate, μ the plastic viscosity and $\tau_y(E,\phi)$ is the field-dependent yield stress, E the electric field and ϕ the particle volume fraction. ER fluid applications, in both shear and flow modes, have been successfully modeled using Eq.1 and it has been demonstrated that experimental results align well with this model [12–14].

For regular yield stress fluids, knowledge of the rheological constitutive relation in one mode can be used to predict the flow performance in a different mode. However, recent studies [12, 15, 16] have indicated that there is a difference in the dynamic response of ER fluids in shear and flow modes. Lee et al. [12] have compared the Bingham properties of an ER fluid in both modes and observed that the Bingham yield stress is higher in flow mode. Nam et al. [15] have studied the dynamic response of an ER fluid in steady pressure-driven flow and found that the response in flow mode is dominated by a densification process, in which the competition between particle interaction and hydrodynamic forces on the incoming particles leads to cluster formation. On the other hand, in shear mode, they note that aggregation of chains into columns is the dominant process. This is

TABLE I. A summary of the different modes of operation of ER devices and their typical engineering applications

Mode of operation	Illustrative schematic	Applications
Shear mode	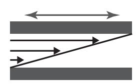	Clutches, brakes, dampers [2, 3]
Flow mode	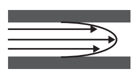	Valves, vibrators [2–6]
Squeeze mode		Shock absorbers, dampers [2, 3]

in agreement with recent studies by Qian et al. [17] on structure evolution in channel flow of ER fluids.

In order to accurately model systems which utilize ER fluids, particularly ER valves, there is a need for a better understanding of how the yield-hardening behavior observed in channel flow, and arising from a change in the microstructure that forms, differs from the rheological response observed in shear mode. Yield-hardening in flow mode is dominated by a densification process, which in turn depends on the initial volume fraction of particles in the fluid. In general, understanding the effect of particle volume fraction on the response of ER fluids has proven to be challenging. For a given electric field, a linear dependence of the yield stress with increasing particle volume fraction has been observed [18–20]. However, at higher volume fractions, some report the presence of a maximum in the yield stress [18, 19] while others observe an exponential-like growth [20]. A first step to resolve this discrepancy is to perform a systematic study comparing the effects of the particle volume fraction on the response of the ER fluid in the two different flow modes.

In the present study, we take this first step by experimentally investigating the yielding properties of ER fluids with different particle volume fractions under both steady simple shear flow and pressure-driven channel flow with a constant electric field. Values of Bingham yield stress are extracted from the data by regression to Eq.1 and a comparison between the fluid responses in these two modes can then be performed. Finally, we present a model that captures the experimentally observed dependence of the fluid rheology on particle volume fraction in shear, as well as a phenomenological model that rationalizes the densification process and consequent yield hardening measured in channel flow. Our interest lies in using these densification models to predict the yield pressure of rapidly-actuated hydraulic devices such as ER valves from viscometric measurements performed on a torsional rheometer.

II. MATERIALS AND METHODS

ER fluids with different particle volume fractions ($0 \leq \phi \leq 0.55$) were prepared from a stock solution of a commercially-available ER fluid (Fludicon, RheOil4). The stock solution has a particle volume fraction $\phi = 0.41$ and is made of a colloidal suspension of polyurethane (PUR) particles doped with Li^+ (mean diameter of 1.4 ± 0.6 m) with silicone oil as a carrier fluid [21–23]. An SEM showing the morphology of the ER particles is shown in the supplementary material (Fig. S1). This class of ER fluids containing polymer particles doped with salt and/or polar organic dopants have been shown to exhibit a low base viscosity and a relatively high yield stress while having low current density. In addition, they also show good sedimentation and re-dispersion properties, a short response time (1-10 ms) and long-term stability making them a promising candidate for practical applications using electrorheological fluids [13, 24]. Particle volume fractions lower than the stock solution were obtained by dilution with 100 cSt silicone oil while higher particle volume fractions were obtained by centrifuging the stock solution and removing a known volume of carrier fluid using a micropipette and then re-suspending the centrifugate using an ultrasonic bath.

The rheological response of the ER fluid under shear mode was measured using an AR1000N stress-controlled rotational rheometer, with a custom-made ER fixture which applies a uniform electric field between two aligned parallel plates. Steady shear flow tests with decreasing shear rates varying from $4 \geq \dot{\gamma} \geq 0.1$ s^{-1} were performed using a parallel-plate geometry with a gap of 300 μm. This procedure, analogous to that described by [25], has been shown to insure that a reproducible value of the dynamic yield stress is reached at steady-state for a similar class of materials. The maximum shear rate applied was chosen to be $\dot{\gamma} \geq 4$s^{-1} to minimize formation of shear-induced lamellar structures during the steady shear flow tests that tend to be associated with a non-monotonic flow curve [7, 8]. This insures that the ER fluid remained homogeneous during the steady shear flow tests and that modeling using the Bingham model (Eq.1) as well as comparison to flow data obtained from microchannels is applicable. The tests were performed at constant temperature $T = 22°$C and constant particle volume fraction $\phi = 0.41$ with different electric fields as well as constant electric field $E = 3$ kV/mm for fluids with different particle volume fractions. The electric field $E = 3$ kV/mm was chosen because it is of particular interest in valve applications: This electric field is high enough for potential engineering applications and for dielectrophoretic effects to be negligible and low enough to avoid electrical breakdown if an air bubble passes through the microchannel.

To measure the rheological response under flow mode, a rectangular microchannel was fabricated [17], (shown in Fig.1). The microchannel consists of three regions: a test section with electrically conductive side walls through

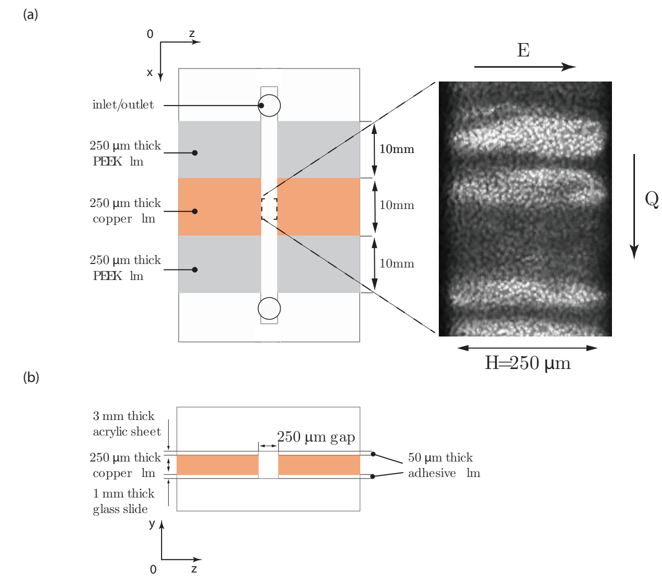

FIG. 1. (a) Schematic of a microchannel fabricated for pressure measurements in flow mode. Also shown is a top view showing the microstructures that develop upon application of an electric field $E = 4$kV/mm for $\phi_0 = 0.02$ (b) Cross-sectional view of the microchannel in the flow direction.

which the field is applied, and two auxiliary sections with non-conductive side walls at the inlet and outlet to minimize effects due to the curvature of the streamlines. The two electrode side walls are made out of a conductive copper film (250 m thick, 10 mm long) and separated by a 250 μm gap. For the non-conductive walls, a polyether ketone film of similar dimensions was used. To seal the microchannel, a 50 μm thick adhesive film (3M, 966) bonded the films to a 1 mm thick glass slide and a 3 mm thick acrylic sheet with tapped holes for the inlet and outlet adapters. The portion of the microchannel, over which an electric field can be applied, has the dimensions $L = 10$ mm, $W = 350$ μm, $h = 250$ μm. The conductive side walls were connected to a high voltage power supply (Stanford Research Systems PS350) via a driver circuit board. ER fluids were injected into the channel using a gas-tight glass syringe (Hamilton, 1005TLL) that was connected to the microchannel with stainless steel tubing (ID=1.6 mm). The flow rate Q, of the fluid was controlled by a syringe pump (Harvard Apparatus, PHD Ultra) and operated within the range of $30 \leq Q \leq 60$ μL/min. The pressure drop between the entry and exit of the channel was measured using a differential pressure sensor (Honeywell, 26PCBFA6D) with a measurement range of $0 \leq \Delta P \leq 35$ kPa; the signal was amplified and acquired using a DAQ board (National Instrument, DAQ1200).

III. RESULTS AND DISCUSSION

Flow curves of the measured shear stress vs. imposed shear rate curves, for the stock solution ($\phi = 0.41$) at different electric fields, obtained in shear mode are presented in Fig.2 and the data was fit with the Bingham model (Eq.1). We observe that in the absence of an electric field, the ER fluid behaves like a Newtonian fluid of viscosity $\mu = 31$ mPa.s. When an electric field is applied for E1.5 kV/mm , the ER fluid develops a field-dependent yield stress as shown in Fig.2b.

The flow curves for the solutions with different particle volume fractions at $E = 3$ kV/mm, obtained in shear mode are presented in Fig.3. This data was fit with the Bingham model of Eq.1. While some applications operate at high shear rates with an electric field applied (e.g. dampers and vibration control devices), for valve applications, our interest lies solely in the yield pressure of the valve and thus in the shear yield stress extracted from the Bingham model fit. For each volume fraction, the Bingham yield stress was extracted from the fit to be compared to the yield stress obtained from flow mode measurements. Fig.4 shows a sample output for the pressure drop measured in a flow-mode experiment as a function of time at two different particle volume fractions ($\phi = 0.05, 0.4$) with an imposed flow rate $Q = 50$ μL/min. The observed curves all indicate an initial pressure rise followed by a series of oscillations. At the beginning of each test, the electric field is activated causing the ER fluid initially present in the microchannel to block the flow. As the syringe pump displaces the fluid, the effective "lumped" compressibility β of the entire microfluidic system (consisting of the syringe, tubing, channel and fluid contained therein) comes into play and the pressure rises. For a given flow rate, the slope of the pressure rise is the same for different volume fractions and can be used to estimate this lumped compressibility β of the system ($\beta = 5$ MPa $- 1$). When the imposed pressure difference exceeds a critical value, the ER microstructure yields, enabling the ER suspension to flow, thereby resulting in a drop in pressure. Since the electric field is still present in the channel, at a second critical pressure, the flow is arrested once more and the compression cycle starts again, hence the observed oscillations. By averaging over a series of peaks, we obtain an average value of the yield pressure differential for the channel at each imposed mass flow rate. In the lubrication limit ($L \gg h, W$), the field-dependent pressure difference at yield $\Delta P(E, \phi)$ can be related to the Bingham yield stress using the following relation obtained via a global force balance on the system [17, 26]:

$$\Delta P(E, \phi) = \frac{2\tau_y L(h + W)}{hW} \tag{2}$$

where L is the length of the channel over which the field is applied and h is the gap between the electrodes. Using this relation, we can compute the Bingham yield stress $\tau_y(E, \phi)$ from the measured yield pressure for each flow

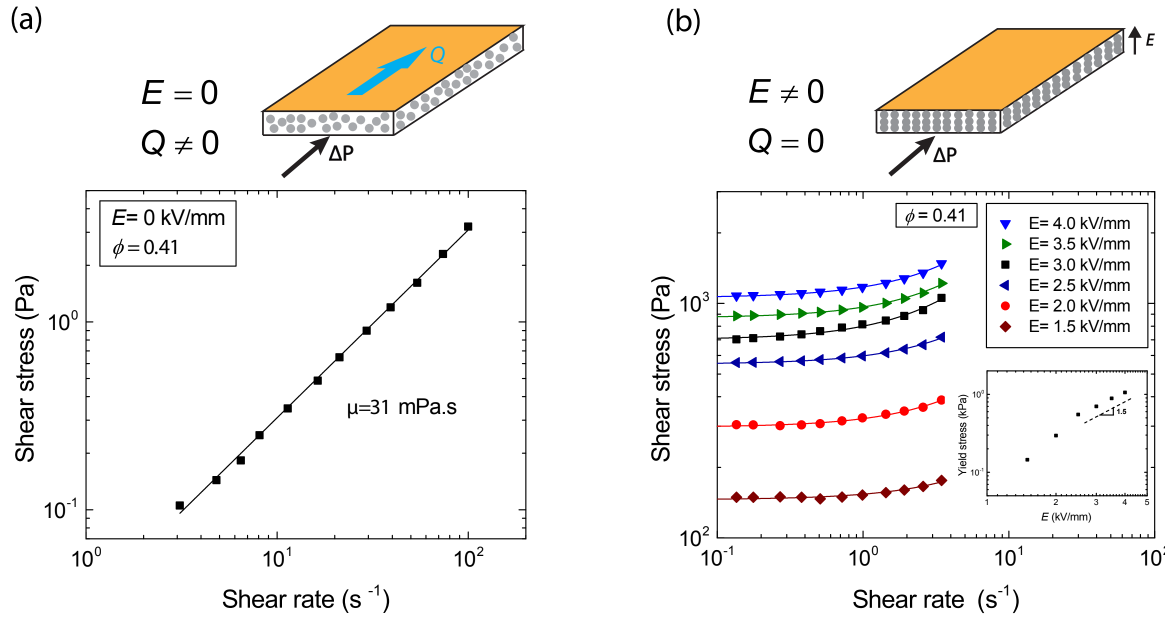

FIG. 2. Shear stress vs. shear rate curves for different electric fields obtained from steady shear flow tests on the AR1000N rheometer with a custom ER parallel plate fixture (R = 20 mm, H = 0.3 mm) for ϕ = 0.41. The lines indicate fits of the data with the Bingham model [Eq. 1]. a) Field off case (E = 0 kV/mm): The ER fluid is Newtonian and flows through the microchannel b) Field on case ($E > 0$ kV/mm): The ER fluid has a field-dependent yield stress and flow can only occur in the microchannel if the applied pressure drop exceeds the yield pressure drop.

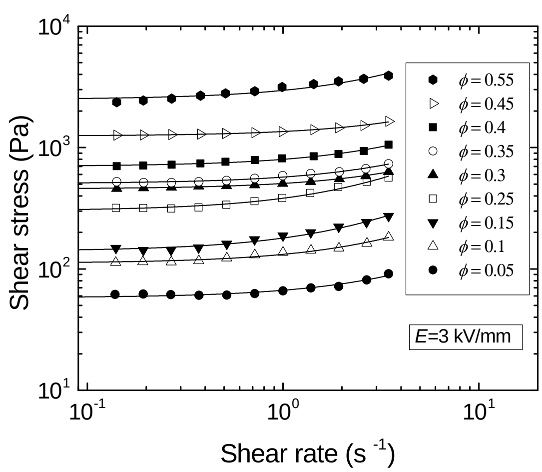

FIG. 3. Shear stress vs. shear rate curves for different particle volume fractions obtained from steady shear flow tests on the AR1000N rheometer with a custom ER parallel plate fixture (R = 20 mm, H = 0.3 mm) at E = 3 kV/mm. The lines indicate select fits of the data with the Bingham model [Eq. 1].

rate and particle volume fraction.

The yield stress data extracted from the tests in shear and flow modes are shown in Fig.5 as a function of the particle volume fraction. We observe that, for all the flow rates tested, the yield stress computed in flow mode is a weak function of the flow rate, but is consistently greater than the one extracted from the steady-shear experiments. In steady shear, the yield stress is found to increase linearly with particle volume fraction at low volume fractions and then more rapidly at higher volume fractions. In channel flow, we observe that after an initial increase the extracted yield stress reaches a plateau value above a composition of $\phi \approx 0.25$. This plateau intersects the yield curve obtained from shear tests at $\phi \approx 0.54$. Electrorheological fluids, as well as yield stress fluids, are prone to slip under shear [27, 28] and control experiments were performed to confirm that the measurements taken represent a true yield of the material and that wall slip does not play a major role in our measurements . Steady shear flow tests performed on the rheometer were done at different gaps [29] and are shown to superimpose for $\phi = 0.41$ and $E = 3$ kV/mm (Fig. S3) indicating that wall slip plays a negligible role in our measurements for the range of shear rates tested. For the case of channel flow, video (supplied in Supplementary Material) taken using the imaging setup described by Qian et al [17]) demonstrates the absence of slip at the walls for a low volume fraction fluid ($\phi = 0.02$) at an applied of field of $E = 4$ kV/mm and an imposed flow rate $Q = 30$ μL/min.

To rationalize these results, we note that in the steady shear experiments, the system is closed and the volume fraction of particles in the sample is fixed; whereas in

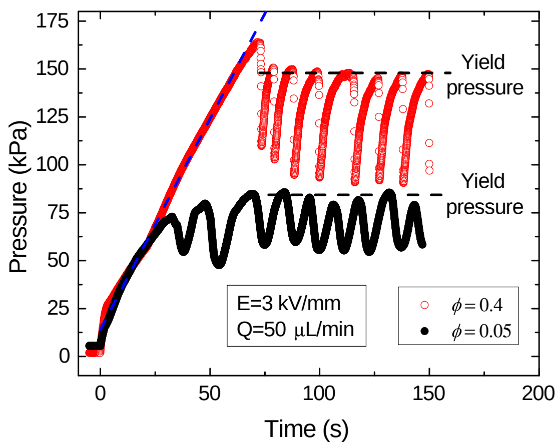

FIG. 4. Pressure drop across the microchannel for two different particle volume fractions ($\phi = 0.05, 0.4$) as a function of time for an electric field of $E = 3$ kV/mm and an imposed flow rate $Q = 50$ μL/min. The dashed lines represent the peaks of the curve which are averaged to determine the yield pressure of the ER valve at each applied field strength, volumetric flow rate and fluid volume fraction. The overall system compressibility β estimated from the slope (blue dotted line) of the pressure rise is $\beta = 5$ MPa^{-1}.

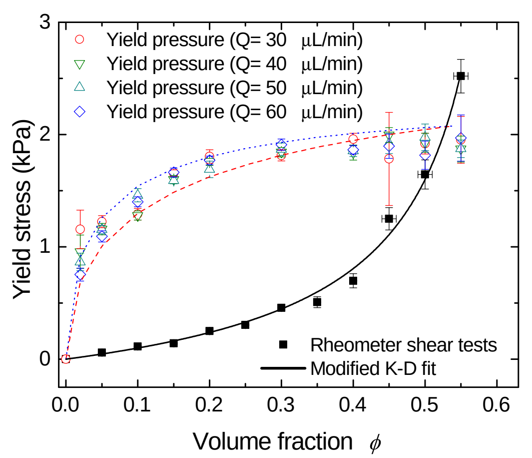

FIG. 5. Comparison of the yield stress extracted from the viscometric tests in the rheometer and from the yield pressure in the microchannel flow setup for flow rates Q ranging from 30-60 μL/min as a function of the particle volume fraction for $E = 3$ kV/mm. The black solid line shows the fit of the modified Krieger-Dougherty model [Eq. 4] to the viscometric data. The red and blue dashed lines show the fit of the proposed model with the microchannel data for $Q = 30$ μL/min and $Q = 60$ μL/min respectively.

channel flow, the system is open and new particles are continuously convected into the microchannel thus potentially increasing the local volume fraction if the fluid exiting the channel is depleted in particles. Since the yield strength of the ER fluid is determined by its microstructure, which in turn depends on the local volume fraction of particles, the higher value of yield stress observed in channel flow, and the saturation of the yield stress at higher volume fractions, are both consistent with an increase of the local volume fraction in the channel to a maximum value of $\phi_M \approx 0.54$. These results are consistent with the densification process described qualitatively by Nam et al. [15] and the images taken by Tang et al. [8] and Qian et al. [17] showing cluster formation in channel flow and the associated increase in volume fraction.

A. Modeling the yield stress in wall-driven shear flow

In a wall-driven shear flow with a homogeneous orthogonal electric field, the measured yield stress is a material function that depends solely on the electric field and the volume fraction of particles. Our focus is to model the effect of the volume fraction of particles on the yield stress of ER fluids in wall-driven flows.

Previous studies have shown that the yield stress of ER fluid in wall-driven shear flow exhibits a maximum [18, 19], while others show a monotonic increase of the yield stress with volume fraction [30–32]. In our case, no maximum in yield stress was observed within the range of volume fractions studied. Based on the chain model, the influence of the particle volume fraction on the yield stress of ER fluids is often described using a power law or exponential model over the volume fractions studied [19, 20, 33]. These models fail to capture the effects observed here, namely a linear dependence at low volume fractions and a diverging behavior as the volume fraction approaches the maximum packing fraction (expected to be $\phi = 0.64$ for a random close packing of spherical monodisperse particles). The observed results are more akin to results obtained for concentrated suspensions of solid particles in yield stress fluids. For such suspensions, the viscometric properties (viscosity, shear modulus, yield stress) are often modeled using an empirical Krieger-Dougherty model [34–36]:

$$\frac{\tau_y(\phi)}{\tau_0} = (1 - \frac{\phi}{\phi_m})^{-K\phi_m} \tag{3}$$

where K is a coefficient that quantifies the initial linear increase in yield stress at low volume fractions, τ_0 is a characteristic yield stress and ϕ_m is the maximum packing fraction. K is analogous to the Einstein coefficient or intrinsic viscosity when the shear viscosity of a suspension is fitted to this model. We propose to model the influence of the particle volume fraction on the yield stress of the ER fluid by using a modified form of this relationship to account for the absence of a yield stress when no particles are present ($\phi = 0$) :

$$\frac{\tau_y(\phi)}{\tau_0} = \left[(1 - \frac{\phi}{\phi_m})^{-K\phi_m} - 1\right] \tag{4}$$

A fit of this model to the yield stress in shear vs. volume fraction curve is shown in Fig.5 with $R^2 = 0.98$ for $K = 1.23$, $\tau_0 = 700$ Pa and ϕ_m=0.63. A similar model was used by Mueller et al. [37] and Heymann et al. [38] to fit the yield stress of suspensions of solid spheres with $K\phi_m = 2$. We expect that this divergence from the case of solid suspensions is due to the fact that ER fluids are active materials that do not exhibit a yield stress in the absence of an electric field, but rather develop this property through the aggregation of particles into chains and columns [4, 15] and can form ordered lamellar structures upon the application of the electric field [7, 8].

B. Modeling the yield stress in channel flow

As discussed, ER fluid flow in a channel is characterized by a densification process that is manifested as an increase in the local volume fraction of particles in the channel and in the overall pressure differential. Unlike wall-driven flow, the measured yield function is not a material property of the fluid but rather a complex function of the fluid and channel properties. Consider an ER fluid of initial volume fraction ϕ_0 that is pumped at a constant flow rate Q into an ER valve that is activated with a constant transverse electric field E. Due to the electrostatic interactions, stable microstructures are formed in the channel through chaining and aggregation of particles. Eventually, these particulate chains may span the channel width and then become immobilized in the channel while the suspending solvent continues to flow out of the channel exit. The evolution of the structures formed during flow, and thus the particle volume fraction in the channel, is a complex function of ϕ_0, Q and E.

We characterize the structures formed in the ER channel using the concept of hydraulic permeability κ which must satisfy the following conditions as shown in Fig.6. First, at large flow rates $Q \to \infty$ or small initial volume fraction $\phi_0 \to 0$, all structures are unstable as the hydrodynamic forces acting on the chains dominate over the electrostatic forces. We expect no particles to be retained in the channel and thus a flow mobility $M_0 = \frac{\Delta P}{Q}$ that is given by standard equations for viscous flow in a channel. Under the lubrication approximation $W \gg h$, $M_0 = \frac{Wh}{12\mu}$ where h is the electrode thickness (which forms the channel separation), W the width of the channel and μ the viscosity of the fluid. The flow mobility can be related to an effective permeability κ_0 via the Darcy equation for flow in porous media and we can define the permeability in this limit as $\kappa_0 = M_0\mu$. Second, in the limit $Q \to 0$, hydrodynamic forces are small and the particles reach a maximum packing volume fraction ϕ_M and the chained

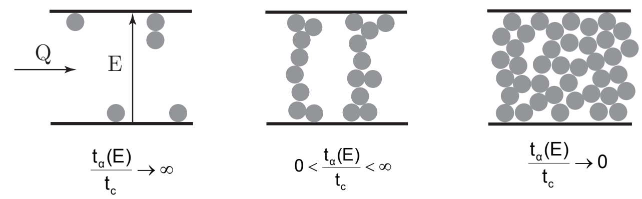

FIG. 6. Schematic of the chained microstructures built in the channel as a function of the non-dimensional ratio of the aggregation time $t_\alpha(E)$ to the convective time $t_c = \frac{LA}{Q}\frac{(\phi_M - \phi_0)}{\phi_0}$. As the ratio $\frac{t_\alpha(E)}{t_c}$ gets smaller, the residence time in the channel becomes longer, there is less frustration and the structures can anneal to a higher packing fraction ϕ_M.

microstructure that is formed by the ER suspension has a permeability κ_M. We note that the structure formed under dynamic flow conditions may be trapped at a maximum packing volume fraction ϕ_M that is lower than the maximum possible packing fraction reached under static conditions ϕ_m. These conditions are in agreement with the experimental observations of Tang et al. [8]) and Nam et al [15] that show that cluster size observed in channel flow decreases with the imposed flow rate. The existence of several time scales in the evolution of the structure of ER fluids has been shown in previous reports [8, 15, 17, 39, 40]: a short time scale related to the aggregation of particles into chains and a longer time scale associated with cluster formation. Following the work by Qian et al. [17], the electric field sets a time scale for aggregation $t_\alpha(E)$ while the structure formation is governed by the ratio of the convective time scale for the flowing suspension t_c to the aggregation time scale $t_\alpha(E)$. The convective time scale t_c is given by $t_c = \frac{LA}{Q}\frac{(\phi_M - \phi_0)}{\phi_0}$ and represents the time needed to fill a channel of length L and cross-section A to the maximum volume fraction ϕ_M when starting from an initial volume fraction ϕ_0.

We propose the following permeability function κ_s that defines the overall microstructure formed within the channel.

$$\kappa_s = \kappa_M + (\kappa_0 - \kappa_M)(1 - e^{-\frac{t_\alpha(E)}{t_c}}) \tag{5}$$

This function satisfies the experimental observations described above and physically corresponds to the fact that under fast flow rates or small initial volume fractions, the structure formed will be more permeable than at slow flow rates. As the flow rate is reduced, the suspended particles have more time to rearrange and reach the maximum packing fraction ϕ_M without getting trapped in a frustrated or jammed state at a lower volume fraction. An analogous functional form was proposed by Nakano et al. [16] to model the dependence of the pressure drop for flow of ER fluids in a rectangular channel on the flow rate, and shown to agree with their experimental results.

To relate permeability and average volume fraction in the channel at any given time, we use the simple relation proposed by Qian et al. [17]

$$\kappa = \kappa_0(1-\phi)^n \tag{6}$$

where ϕ is the average volume fraction in the channel and n is an empirical parameter found to be $n = 6$ by Qian et al [17]. This functional form is chosen because it was shown experimentally that it provides a good approximation to the evolution of the permeability in an ER channel. In addition, it is readily invertible thus providing an exact expression for the average volume fraction of particles in the channel for a given permeability. A more in depth discussion, comparing permeability models from the literature and this model, is provided in the Supplementary Information section. Combining equations 5 and 6, we can compute the average volume fraction of the assembled microstructures built in the channel ϕ_s :

$$\phi_s(E,Q,\phi_0) = 1-\left[\frac{\kappa_M}{\kappa_0}+\left(1-\frac{\kappa_M}{\kappa_0}\right)\left(1-e^{-\frac{t_\alpha(E)}{t_c}}\right)\right]^{\frac{1}{n}} \tag{7}$$

The yield stress of the permeable microstructure that assembles in the channel is then given by $\tau_y(\phi_s)$ where $\tau_y(\phi)$ is the material function that was measured independently under wall-driven shear flow in the rheometer and discussed earlier in Eq.4.

Fig.5 shows the experimental data and the model predictions in our channel geometry for $t_\alpha(E) = 3.5$ ms and a maximum packing fraction $\phi_M = 0.54$ for two different flow rates: 30 and 60 μL/min. The model demonstrates the ability to capture the experimental observation discussed earlier for ER fluids in pressure-driven microchannel flow: a sharp increase of the yield stress with low initial volume fractions, followed by saturation at high initial volume fractions and a weak dependence of the measured results on the flow rate. The fitted value found for the aggregation time scale $t_\alpha(E) = 3.5$ ms is within the range reported in the literature for electrorheological fluids [5, 13, 15, 19]. The analysis performed does not depend sensitively on the choice of the permeability model provided the permeability of the chained microstructure in the channel is a monotonically decreasing function of particle volume fraction (as would be expected). This simple two-parameter phenomenological model, thus offers a simple, yet rich, physical mechanism to model the yield hardening observed in channel flow. Previous work has focused on showing that each mode of shear has to be characterized separately experimentally to model the performance of ER fluids in devices of interest. Using this model and the physical understanding of the densification that occurs in channel flow, we have demonstrated that we are able to model and predict the rheological performance in channel flow using a characterization of the dependence of the yield stress on particle volume fraction performed in wall-driven flow (Eq.4) and allowing us to reconcile the discrepancies observed in the two modes of flow.

IV. CONCLUSIONS

In summary, when designing devices such as actuators or valves that use active suspensions such as electrorheological or magnetorheological fluids in flow mode, the phenomenon of yield hardening, due to the local densification in the suspension microstructure reported here, must be considered and taken into account in the systems modeling. In the present work, we have shown that the complex interdependencies between the electrostatic interactions, the hydrodynamic forces and the channel geometry can be modeled by understanding the ratio of the particle aggregation time scale to the convective flow time scale and linked to the permeability of the chained microstructures that assemble in the channel, when a transverse electric field is applied to the flow. The understanding of flow-induced densification and saturation is important in optimizing parameters such as channel length and switching time in ER-fluidic valve design. With the physical understanding of the densification that occurs in channel flow, we can model and predict the performance in channel flow using a characterization of the dependence of the yield stress on particle volume fraction performed in wall-driven flow, thus allowing us to reconcile the discrepancies observed in the two modes of flow.

ACKNOWLEDGMENTS

This work was supported by the DARPA Maximum Mobility and Manipulation (M3) program. The authors would like to thank Mike Murphy, Marc Strauss and Robert Playter at Boston Dynamics and Maria Telleria for their helpful discussions and insights.

[1] W. M. Winslow, Journal of Applied Physics **20**, 1137 (1949).
[2] R. Stanway and J. L. Sproston, Journal of Dynamic Systems, Measurement, and Control **116**, 498 (1994).
[3] J. P. Coulter, K. D. Weiss, and J. D. Carlson, Journal of Intelligent Material Systems and Structures **4**, 248 (1993).
[4] D. J. Klingenberg and C. F. Zukoski, Langmuir **6**, 15 (1990).
[5] X. Niu, W. Wen, and Y.-K. Lee, The 13th International Conference on Solid-State Sensors, Actuators and Microsystems, 2005. **1**, 652 (2005).
[6] K. Yoshida, M. Kikuchi, J. H. Park, and S. Yokota, Sensors and Actuators, A: Physical **95**, 227 (2002).
[7] J. G. Cao, J. P. Huang, and L. W. Zhou, Journal of Physical Chemistry B **110**, 11635 (2006).
[8] X. Tang, W. H. Li, X. J. Wang, and P. Q. Zhang, International Journal of Modern Physics B **13**, 1806 (1999).

[9] Y. Pappas and D. J. Klingenberg, Rheologica Acta **45**, 621 (2006).
[10] R. Tao, Journal of Physics: Condensed Matter **13**, R979 (2001).
[11] Y. Tian, X. Zhu, J. Jiang, Y. Meng, and S. Wen, Smart Materials and Structures **19**, 105024 (2010).
[12] H. G. Lee and S. B. Choi, Materials & Design **23**, 69 (2002).
[13] M. Gurka, R. Petricevic, S. Schneider, and S. Ulrich, Journal of Intelligent Material Systems and Structures **22**, 1745 (2011).
[14] Y. J. Jang, M. S. Suh, M. S. Yeo, and S. B. Choi, Journal of Intelligent Material Systems and Structures **7**, 604 (1996).
[15] Y. J. Nam, M. K. Park, and R. Yamane, Experiments in Fluids **44**, 915 (2008).
[16] M. Nakano, R. Aizawa, and Y. Asako, International Journal of Modern Physics B **10**, 2965 (1996).
[17] B. Qian, G. H. McKinley, and A. E. Hosoi, Soft Matter **9**, 2889 (2013).
[18] R. T. Bonnecaze and J. F. Brady, Journal of Rheology (1978-present) **36**, 73 (1992).
[19] T. Hao, *Electrorheological Fluids The Non-aqueous Suspensions*, edited by Science (Elsevier, 2005) pp. 152–234.
[20] Z. Song, Y. Cheng, J. Wu, J. Guo, and G. Xu, Applied Physics Letters **101**, 23 (2012).
[21] ERF Production Würzburg GmbH Product Information on RheOil 4.0, http://www.erfgmbh.de (2008).
[22] Y. Reichert and H. Böse, in *Electro-Rheological Fluids and Magneto-Rheological Suspensions* (World Scientific, 2011) pp. 338–347.
[23] S. Schneider and S. Eibl, Applied Rheology **18**, 23956 (1 (2008).
[24] M. Gurka, L. Johnston, and R. Petricevic, Journal of Intelligent Material Systems and Structures **21**, 1531 (2010).
[25] G. Ovarlez, S. Cohen-Addad, K. Krishan, J. Goyon, and P. Coussot, Journal of Non-Newtonian Fluid Mechanics **193**, 68 (2013).
[26] R. B. Bird, R. C. Armstrong, and O. Hassager, *Related Information: Fluid Mechanics. Dynamics of Polymeric Liquids. Volume 1. 2nd Edition* (1987) p. Medium: X; Size: Pages: 784.
[27] S. Schneider, International Journal of Modern Physics B **26**, 1250006 (1 (2012).
[28] R. Buscall, Journal of Rheology (1978-present) **54**, 1177 (2010).
[29] A. Yoshimura and R. K. Prud'homme, Journal of Non-Newtonian Fluid Mechanics **32**, 53 (1988).
[30] X. D. Pan and G. H. McKinley, Langmuir **14**, 985 (1998).
[31] C. J. Gow and C. F. Zukoski IV, Journal of Colloid and Interface Science **136**, 175 (1990).
[32] L. Marshall, C. F. Zukoski, and J. W. Goodwin, Journal of the Chemical Society, Faraday Transactions 1 **85**, 2785 (1989).
[33] K. P. S. Parmar, Y. Méheust, B. Schjelderupsen, and J. O. Fossum, Langmuir **24**, 1814 (2008).
[34] I. M. Krieger and T. J. Dougherty, Transactions of The Society of Rheology (1957-1977) **3**, 137 (1959).
[35] X. Chateau, G. Ovarlez, and K. L. Trung, Journal of Rheology (1978-present) **52**, 489 (2008).
[36] M. Kogan, L. Ducloué, J. Goyon, X. Chateau, O. Pitois, and G. Ovarlez, Rheologica Acta **52**, 237 (2013).
[37] S. Mueller, E. W. Llewellin, and H. M. Mader, Proceedings of the Royal Society of London A: Mathematical, Physical and Engineering Sciences **466**, 1201 (2010).
[38] L. Heymann, S. Peukert, and N. Aksel, Rheologica Acta **41**, 307 (2002).
[39] B. Abu, Journal of Physics: Conference Series **412**, 012009 (1 (2013).
[40] J. C. Hill and T. H. V. Steenkiste, J. Appl. Phys. **70**, 1207 (1991).
[41] S. Ergun, Chemical Engineering Progress **48**, 89 (1952).
[42] A. Tamayol and M. Bahrami, Physical Review E - Statistical, Nonlinear, and Soft Matter Physics **83**, 1 (2011).
[43] P. C. Carman, Transactions, Institution of Chemical Engineers, London **15**, 150 (1937).
[44] J. Kozeny, Sitzungsber Akad. Wiss., Wien **136**, 271 (1927).